ACS OMEGA

http://pubs.acs.org/journal/acsodf

Article

Layer-by-Layer Self-Assembly of Polyelectrolytes on Superparamagnetic Nanoparticle Surfaces

Zied Ferjaoui, Sara Nahle, Crosby Soon Chang, Jaafar Ghanbaja, Olivier Joubert, Raphaël Schneider, Luc Ferrari, Eric Gaffet, and Halima Alem*

Cite This: *ACS Omega* 2020, 5, 4770−4777

Read Online

ACCESS | Metrics & More | Article Recommendations | Supporting Information

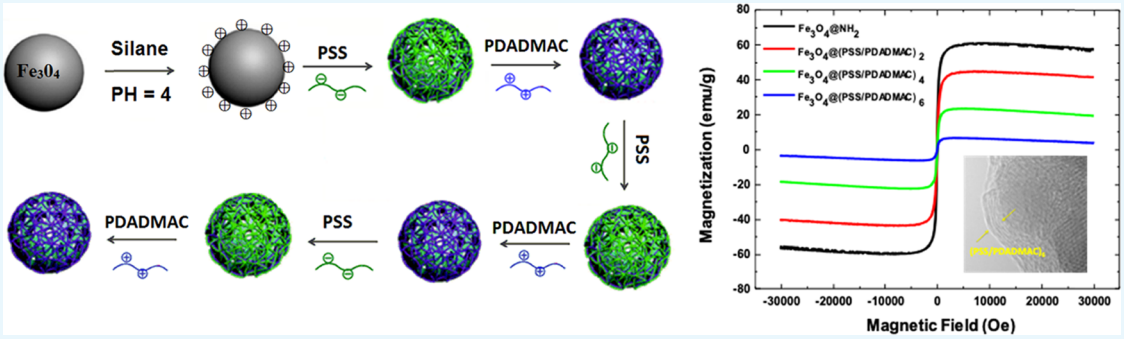

ABSTRACT: Designing and manufacturing multifunctional nanoparticles (NPs) are of considerable interest for both academic and industrial research. Among NPs used in this field, iron oxide NPs show low toxicity compared to metallic ones and are thus of high interest for biomedical applications. In this work, superparamagnetic $Fe_{3-\delta}O_4$-based core/shell NPs were successfully prepared and characterized by the combination of different techniques, and their physical properties were investigated. We demonstrate the efficiency of the layer-by-layer process to graft polyelectrolytes on the surface of iron oxide NPs. The influence of the polyelectrolyte chain configuration on the magnetic properties of the $Fe_{3-\delta}O_4$/polymer core/shell NPs was enlightened. The simple and fast process described in this work is efficient for the grafting of polyelectrolytes from surfaces, and thus, derived $Fe_{3-\delta}O_4$ NPs display both the physical properties of the core and of the macromolecular shell. Finally, the cytotoxicity toward the human THP-1 monocytic cell line of the core/shell NPs was assessed. The results showed that the polymer-capped $Fe_{3-\delta}O_4$ NPs exhibited almost no toxicity after 24 h of exposure at concentrations up to 25 μg mL^{-1}. Our results show that these smart superparamagnetic nanocarriers with stealth properties are promising for applications in multimodal cancer therapy, including drug delivery.

INTRODUCTION

Owing to their numerous and promising applications, superparamagnetic iron oxide NPs (SPIONs) have attracted the interest of many research groups worldwide.[1−5] In the medical field, their development was shown to be of particular interest as their superparamagnetic behavior guarantees a high magnetization when submitted to a magnetic field, whereas no magnetic remanence can be observed after their exposure to the magnetic field.[6]

The use of SPIONs in the medical field requires their full stability in biological fluids to take advantage of their physical properties. Indeed, when bare iron oxide NPs are dispersed in complex media like physiological fluids, their surface can be altered and the release of Fe^{2+} ions leads to the loss of their physical properties and to the increase of their cytotoxicity.[7] Thus, strategies such as the preparation of core/shell NPs were developed to graft a surrounding layer on the NPs to prevent the adsorption of undesirable molecules or proteins that may alter NP physical properties.[6,8] Moreover, the shell can ensure the passivation of the NP surface for the full preservation of their magnetic properties.[3,6,9] Finally, it is possible to synthesize NPs with new physical and colloidal properties such as magnetic and optical that could not be obtained if each nanomaterial was used separately.[6] Among these strategies, the most commonly used consists of the synthesis of inorganic/inorganic core/shell NPs in which the core is surrounded by a shell composed of at least one layer.[8,10−14] For example, these new nanomaterials could display magnetic and luminescence properties, or if the shell is composed of a porous silica layer,[15−17] drugs could be loaded and released in the cell environment.[14,18] Another method consists of grafting a

Received: September 11, 2019
Accepted: February 10, 2020
Published: March 3, 2020

polymer layer at the surface of SPIONs to enhance their stealth properties in the body[11,19−21] or to combine the magnetic properties of the core and polymer chain physicochemical properties to elaborate responsive NPs that exhibit high potential as drug carriers for cancer therapy.[12,22,23] The previously described strategy leads to very promising nanomaterials especially for cancer therapy by combining imaging and drug release properties. However, the synthetic processes developed to obtain such NPs are time-consuming, and for the more sophisticated ones, the ease of implementation required by industries is hindered.

To overcome the synthetic process limitations, the layer-by-layer (LbL) assembly of charged molecules has shown interesting features.[24] This method consists of the alternative adsorption of charge macromolecules (mainly polyelectrolytes) onto surfaces.[24] It has been shown three decades ago that the process can be versatile, controlled at the nanometer scale, and could eventually lead to structured surfaces with high potential for biological applications.[25]

To the best of our knowledge, the LbL process is usually used for the encapsulation of drugs,[26−30] beds,[31,32] silica nanostructures,[33−35] or iron oxide NPs,[26,36−38] but the synthesis of core/shell NPs was rarely reported.[13,39−42] Palomec-Garfias et al. synthesized magnetic core/shell NPs composed of a γ-Fe_2O_3 core on which were layer-by-layer assembled poly(styrene sulfonate) (PSS) followed by either poly(allylamine hydrochloride) (PAH) or chitosan (Chi).[13] The authors have focused their studies on the influence of the pH on the shell shape, which is directly related to the pH-responsive behavior of the PAH or Chi, which are weak polyelectrolytes.[43] However, the influence of the polyelectrolyte multilayer films on the magnetic properties was not evidenced. In another work devoted to biomedical applications, Mancarella et al. have assembled on $Fe_{3-\delta}O_4$ surfaces biocompatible and biodegradable polymers, that is, poly-L-lysine and dextran, to obtain magnetic curcuma nanocarriers. The curcuma loading and release were monitored, and its triggering by the degradation of the polymer in physiological media was demonstrated.[39] When the curcuma-loaded NPs were made in contact with SKOV-3 ovarian cancer cells, an increase in cell death of about 10% after 48 h of incubation was observed compared to the nude $Fe_{3-\delta}O_4$ NPs.

When the LbL is conducted on flat surfaces, the complete characterization of the multilayered film can be conducted in terms of thickness and organization by different techniques ranging from the UV−visible absorption measurements to X-ray and neutron reflectivity,[24] which gave rise to a better understanding of the film formation. All the experimental conclusions were associated with theoretical studies to fully understand the mechanism of the multilayered film formation depending on the macromolecule properties (M_n, I_p, repetitive unit chemical structure, charge degree).[24] Concerning the adsorption of polyelectrolytes at the surface of NPs, the full characterization of the nanostructure is still lacking due to the spherical shape of the substrates. In this work, we have first developed a process to functionalize magnetic NPs by synthetic and well-described couples of polyelectrolytes:poly(styrene sulfonate)/poly(diallyldimethylammonium chloride) $(PSS/PDADMAC)_n$ (n = number of bilayers) via the LbL process transposed to superparamagnetic $Fe_{3-\delta}O_4$ NPs. After the optimization of the LbL deposition at the NP surfaces, the core/shell NPs were fully characterized, and the use of high-resolution transmission electron microscopy (HR-TEM) evidenced the layered structure of the shell. The influence of the shell thickness on the magnetization properties of the NPs was also investigated. Finally, a cytotoxicity study was conducted using the human monocytic THP-1 cell line, which is involved in the defense against foreign bodies such as NPs. Results showed that the core/shell NPs exhibit low cytotoxicity up to concentrations of 25 μg mL^{-1} toward the THP-1 cell line. The method developed to control the LbL assembly of PSS/PDADMAC on the surface of $Fe_{3-\delta}O_4$ NPs could pave the way for new nanoparticulate systems for biological applications.

RESULTS AND DISCUSSION

To study the efficiency of the LbL assembly of polyelectrolytes at the surface of the $Fe_{3-\delta}O_4@NH_3^+$, we have combined complementary characterization methods to study the microstructures of the core/shell NPs and their colloidal stability after the LbL assembly of PSS and PDADMAC (Figure 1).

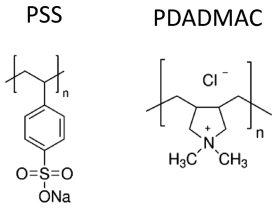

Figure 1. Chemical structures of poly(styrene sulfonate) (PSS) and poly(diallyldimethylammonium chloride) (PDADMAC).

Core/Shell NP Microstructure. To ensure that the process does not damage the crystallinity of the NP core, X-ray diffraction (XRD) experiments were performed. The characteristic diffraction peaks at 2θ = 30.10, 35.60, 43.14, 53.49, 57.11, and 62.88° remain unchanged after the functionalization process and match with the characteristic diffraction (220), (311), (400), (422), (511), and (440) planes of the magnetite Fe_3O_4 phase (JCPDS PDF No. 00-019-0629) (Figure S1 in the Supporting Information).

High-resolution TEM micrographs show the spherical shape of $Fe_{3-\delta}O_4@(PSS/PDADMAC)_6$ NPs (Figure 2). The core displays an average diameter of 10 ± 1.5 nm as determined from TEM images (Figure 2c). The diameter range size of these NPs is well compatible with the expected superparamagnetic behavior at room temperature.[47]

To study the influence of the shell on the physical and colloidal properties of the core/shell NPs and on their cytotoxicity, the coverage of the core by the polyelectrolyte film is necessary. To demonstrate the efficiency of our process, Energy-Filtered TEM analyses were conducted, and an amorphous layer essentially composed of carbon (see the C mapping, Figure 3c) at the surface and at the interspace between particles was observed (Figure 3a−c). The C mapping (carbon is essentially derived from the polyelectrolyte multilayered film) demonstrates that the LbL process enables a full and homogeneous coverage of the core/shell NPs by the polyelectrolytes. Moreover, HR-TEM images show the layered nanostructuration of the $(PSS/PDADMAC)_6$ film as can be seen in the inset of Figure 3d. A final thickness of the polyelectrolyte multilayered film after 6 deposition cycles of about 2.2 nm was calculated from HR-TEM images, which is close to the thickness determined when the process is

https://dx.doi.org/10.1021/acsomega.9b02963
ACS Omega 2020, 5, 4770−4777

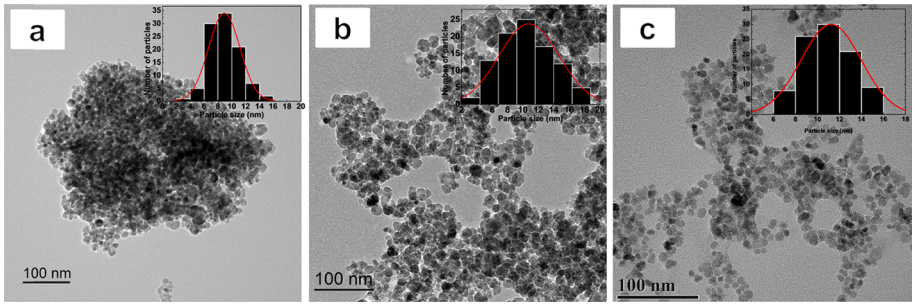

Figure 2. Bright-field TEM micrographs of (a) $Fe_{3-\delta}O_4$ NPs, (b) $Fe_{3-\delta}O_4$@Silane, and (c) $Fe_{3-\delta}O_4$@(PSS/PDADMAC)$_6$. The insets show the size distributions as measured by TEM.

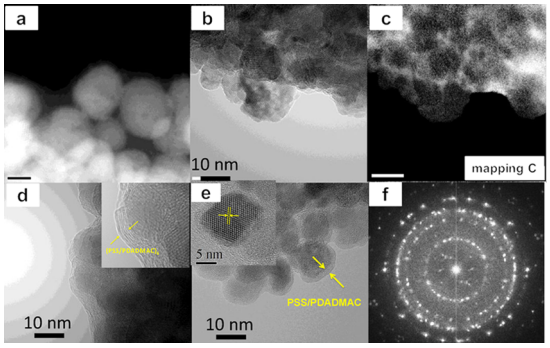

Figure 3. (a) HAADF STEM micrograph of $Fe_{3-\delta}O_4$@(PSS/PDADMAC)$_6$, (b) zero-loss TEM image of $Fe_{3-\delta}O_4$@(PSS/PDADMAC)$_6$, (c) carbon mapping (white areas are rich in carbon) of $Fe_{3-\delta}O_4$@(PSS/PDADMAC)$_6$, (d,e) HR-TEM micrographs of $Fe_{3-\delta}O_4$@(PSS/PDADMAC)$_6$, and (f) selected area electron diffraction of $Fe_{3-\delta}O_4$@(PSS/PDADMAC) NPs.

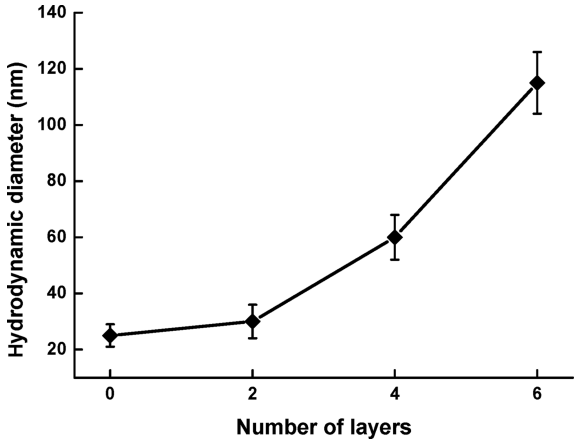

Figure 4. Hydrodynamic diameter of (PSS/PDADMAC)-modified $Fe_{3-\delta}O_4$ NPs dispersed in water determined by DLS.

conducted on flat surfaces.[25] This indicates that the curvature of the surface does not have an impact on the LbL process.

The toxicity of NPs relies on different factors such as size, surface charge, composition, impurities, and specific surface area.[7,48] NP size plays a key role as it affects their uptake by cells, their interaction with organelles, the death mechanism, and their clearance. Indeed, when considering cancer therapeutic nanosystems, it has been shown that NPs have to display sizes between 10 and 200 nm to accumulate into tumors while avoiding healthy tissues owing to their enhanced permeability and retention effect.[22,49]

The average hydrodynamic diameters (D_H) of NPs were measured at each two adsorbed (PSS/PDADMAC) bilayers by dynamic light scattering (DLS) as presented in Figure 4. As expected, the NP hydrodynamic diameters increase with the number of bilayers; that is, $Fe_{3-\delta}O_4$@(PSS/PDADMAC)$_2$, $Fe_{3-\delta}O_4$@(PSS/PDADMAC)$_4$, and $Fe_{3-\delta}O_4$@(PSS/PDADMAC)$_6$ display diameters of 35, 75, and 120 nm, respectively. The increase in capsule shell thickness after the deposition of six PDADMAC/PSS bilayers is ~50 nm, a value that is in good agreement with the data related to the thickness of polyelectrolyte layers adsorbed onto a latex particle determined by single-particle light scattering.[9,16] Due to their sizes varying between 35 and 120 nm, $Fe_{3-\delta}O_4$@(PSS/PDADMAC) NPs are well suited for antitumor treatment.[50,51,54,55]

Iron oxide NPs with diameters below 50 nm exhibit almost no cytotoxity,[48] like ferumoxytol, which is already FDA-approved as an iron supplement. As previously indicated, the surface charge and its density influence the NP toxicity.[52] It has been shown that positively charged particles underwent better cell uptake than negatively charged ones (cationic iron oxide NPs can be more easily ingested by macrophages more easily than anionic ones).

The LbL process is well known to conduct a charge inversion of the substrate at each deposited layer on flat surfaces[53] and will thus lead to changes of NP surface charge. The ζ potential of positively charged $Fe_{3-\delta}O_4$@NH_3^+ NPs at pH 4 is +25 mV (Figure 5). When adding the first layer of PSS, the ζ potential becomes negative and reaches −27 mV, confirming the successful adsorption of the polyanion. The PDADMAC polycation was subsequently assembled onto the negatively charged NPs and leads to the charge inversion of the polarity to +40 mV. As shown in Figure 5, alternating the polycation and polyanion layers induces ζ potential oscillation

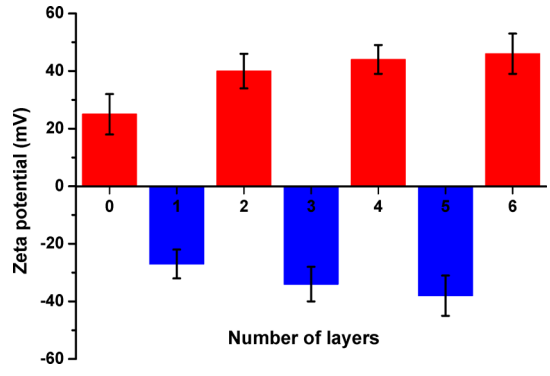

Figure 5. ζ potential values of $Fe_{3-\delta}O_4$@(PSS/PDADMAC)$_n$ NPs as a function of layer number obtained by LbL assembly.

https://dx.doi.org/10.1021/acsomega.9b02963
ACS Omega 2020, 5, 4770−4777

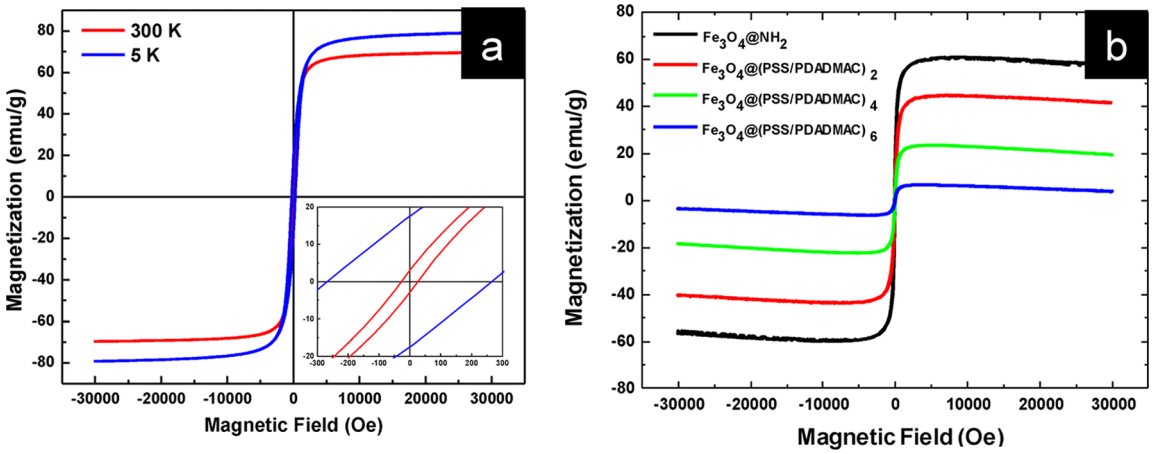

Figure 6. Magnetization curves of (a) $Fe_{3-\delta}O_4$ at 5 and 300 K and (b) $Fe_{3-\delta}O_4$@(PSS/PDADMAC)$_n$ superparamagnetic NPs.

between negative and positive values. The high ζ potential values (up to 40 mV) combined to the HR-TEM measurement, which are close to the thickness measured for the polyelectrolyte layer on their stretched conformation, indicate that the polymer chains keep their complete stretched conformation while assembling on the NP surface. These characteristics make these NPs good candidates for drug or gene delivery for cancer therapy.

Magnetic Measurements. The magnetic properties of the $Fe_{3-\delta}O_4$ SPIONs and of the $Fe_{3-\delta}O_4$@(PSS/PDADMAC)$_n$ NPs were evaluated at 5 and 300 K (Figure 6). Superparamagnetic behavior of the Fe_3O_4 SPIONs was observed at 300 K with a saturation magnetization around 70 emu/g. At 5 K, a hysteresis cycle can be observed due to the transition to a low-temperature blocked state, with a saturation magnetization of 80 emu/g and a coercive field around 270 Oe.

The saturated magnetization values (per gram of $Fe_{3-\delta}O_4$ content) of $Fe_{3-\delta}O_4$@(PSS/PDADMAC)$_2$, $Fe_{3-\delta}O_4$@(PSS/PDADMAC)$_4$, and $Fe_{3-\delta}O_4$@(PSS/PDADMAC)$_6$ NPs are 40, 20, and 9 emu g^{-1}, respectively. These values are lower than those of the native $Fe_{3-\delta}O_4$@NH_2 NPs (60 emu g^{-1}) (Figure 6b). This originates from a decrease in the magnetic interaction due to the diamagnetic coating according to previous reports.[3,9] Nevertheless, the NPs quickly interact with a magnet (Figure 7). The remanence (M_r) and coercivity (H_c) for $Fe_{3-\delta}O_4$@(PSS/PDADMAC) NPs were close to zero, which is typical for superparamagnetic NPs.[17,18]

To confirm the superparamagnetic behavior of NPs, field-cooling (FC) and zero-field-cooling (ZFC) experiments were performed. The magnetization-dependent temperature was studied at an applied field of 75 Oe in the temperature range between 5 and 400 K (the graphs are depicted in the Supporting Information). The gradual increase of the magnetization for the ZFC and FC curves until their intersection at the blocking temperature (T_B) is linked to the progressive rotation of the magnetization of the blocked magnetic NPs toward the field direction.[56] Above T_B, the magnetization curve slope was inverse, which indicates the free alignment of the NPs with the magnetic field during the measurement. It is worthy to mention that this blocking temperature at 270 K (around −3 °C) is higher than that reported for other iron oxide NPs with close sizes, which suggested that the NPs can be slightly aggregated in the media (Figure S3). Indeed, the presence of dipolar interactions can induce a shift of T_B toward higher temperatures.[3,10] Nevertheless, this specific behavior is

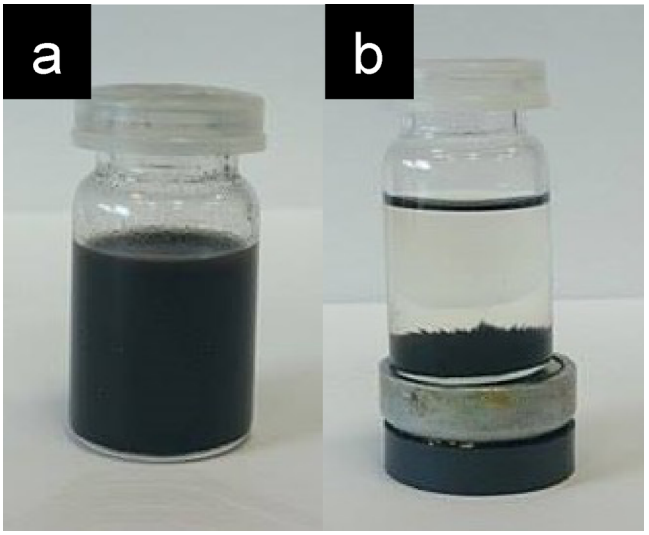

Figure 7. Magnetic separation of $Fe_{3-\delta}O_4$@(PSS/PDADMAC)$_6$ NPs dispersed in water (a) without a magnet and (b) in contact with a magnet.

the fingerprint of superparamagnetism. Moreover, above T_B, the core/shell NPs are superparamagnetic, the $Fe_{3-\delta}O_4$ SPIONs display then superparamagnetic behavior at the room temperature.

The magnetic separation and redispersion process of $Fe_{3-\delta}O_4$@(PSS/PDADMAC)$_6$ NPs is illustrated in Figure 7. The black particles were readily attracted to the bottom of the flask within 10 s by the magnet, and the color of the $Fe_{3-\delta}O_4$@(PSS/PDADMAC)$_6$ solution quickly turned from black to transparent. The particles can be well dispersed again by stirring and ultrasonic vibration.

To envision the applications of these NPs in biological application, cytotoxicity studies were carried out toward THP-1 cells.

Cytotoxicity Study. THP-1 cells are well known to induce an inflammatory reaction when exposed to a drug.[57,58] To evaluate the toxicity of the NPs toward THP-1 cells, cytotoxicity studies of $Fe_{3-\delta}O_4$@(PSS/PDADMAC)$_6$ NPs were conducted by the conventional WST-1 assays. Figure 8 displays the THP-1 viability results after 5 and 24 h of exposure to NPs. Cytotoxicity appears only at 50 μg mL^{-1} and higher doses, and the inhibitory concentration IC_{50} calculated

https://dx.doi.org/10.1021/acsomega.9b02963
ACS Omega 2020, 5, 4770−4777

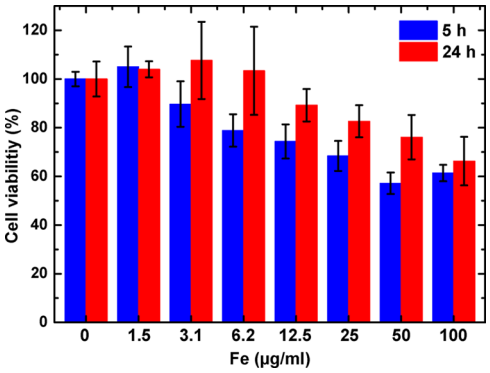

Figure 8. Viability of THP-1 cells after 5 and 24 h of exposure to $Fe_{3-\delta}O_4$@(PSS/PDADMAC)$_6$ NPs.

at 24 h was higher than 100 μg mL^{-1}. This result suggests that iron oxide NP toxicity is low on THP-1 cells and that their induced inflammatory response is limited.[57] According to our results, cell death was less important at 24 h. It may be linked to a mechanism of cell adaptation or to the aggregation of NPs after 24 h, which mitigate their toxicity. However, the cell death observed at high concentrations may originate from the release of reactive oxygen species, which will induce mitochondrial dysfunctions leading to an increase of the swelling and cell permeability and finally to DNA damage.[59,60] However, these NPs still exhibit a favorable low cytotoxicity, which makes them of high interest for biomedical applications.

CONCLUSIONS

In this work, we have provided a novel simple method to encapsulate $Fe_{3-\delta}O_4$ SPIONs by using the LbL approach. The shell construction was followed at each step of the multilayered film formation. The cytotoxic tests toward human cancer THP-1 cells of the core/shell NPs showed that these functional nanomaterials exhibited almost no toxicity at concentrations up to 25 μg mL^{-1}. The techniques reported in this work could be transposed to the LBL of biobased macromolecules like poly-L-lysine and hyaluronic acid for its well-known targeting properties. This work paves the way for the elaboration of new core/shell NPs with promising biomedical properties.

EXPERIMENTAL SECTION

Chemicals. All reagents were purchased from Sigma-Aldrich, except for (3-aminopropyl)trimethoxysilane (Gelest, >95%), poly(sodium 4-styrenesulfonate) (PSS), and poly(diallyldimethylammonium chloride) (PDADMAC), and were used as received.

Synthesis of $Fe_{3-\delta}O_4$ SPIONs. A coprecipitation method was used to synthesize the superparamagnetic $Fe_{3-\delta}O_4$ nanocrystals. 5 mL of a 28% (v/v) aqueous ammonia solution was added to 40 mL of an aqueous mixture of $FeCl_3 \cdot 6H_2O$ (6 mmol; 1.622 g) and $FeSO_4 \cdot 7H_2O$ (5 mmol; 1.39 g). The mixture was stirred and heated at 90 °C under an argon atmosphere.[18] To stabilize the NPs, 15 mL of a 1 M solution of sodium citrate (chosen as the ligand) was added dropwise, and the mixture was stirred for 30 min. The final solution turned black. The SPIONs were recovered by magnetic separation and washed several times with ethanol to remove the unreacted reagents.

Synthesis of (3-Aminopropyl)trimethoxysilane-Coated $Fe_{3-\delta}O_4$ NPs ($Fe_{3-\delta}O_4$@NH_2). (3-Aminopropyl)-trimethoxysilane (0.2 mmol, 49.1 μL) was injected to 10 mL of a homogeneous oxygen-free solution of $Fe_{3-\delta}O_4$ SPIONs (50 mg). After stirring the solution for 2 min, 1 mL of an ethanolic solution of tetramethylammonium hydroxide pentahydrate (TMAH) (0.2 M) was added, and the mixture was further stirred under argon for 15 min at 50 °C. The mixture was then cooled, and $Fe_{3-\delta}O_4$ SPIONs were separated by centrifugation and washed two times with toluene. After the dispersion of the silanized $Fe_{3-\delta}O_4$ SPIONs in 10 mL of toluene, 2 mL of an ethanolic solution of TMAH (36.25 mg) was injected in the media. The mixture was stirred under argon pressure for 30 min at 50 °C. Afterward, the reactor was cooled in a water bath, and $Fe_{3-\delta}O_4$ SPIONs were separated by centrifugation and washed two times with toluene.[44]

Synthesis of $Fe_{3-\delta}O_4$@(PSS/PDADMAC) NPs. After the silanization step, $Fe_{3-\delta}O_4$@NH_2 SPIONs were obtained. Because the layer-by-layer assembly is mainly driven by electrostatic interactions, the pH of the $Fe_{3-\delta}O_4$@NH_2 solution was adjusted to 4 in order to have a highly positively charged surface ($Fe_{3-\delta}O_4$@NH_3^+). The LbL process could then be conducted as follows: the $Fe_{3-\delta}O_4$@NH_3^+ NPs were stirred for 10 min in 10 mL of 10^{-2} M solution of PSS followed by ultracentrifugation. The as-synthesized $Fe_{3-\delta}O_4$@PSS was redispersed in Milli-Q water, stirred for 5 min to remove the physisorbed molecules, and ultracentrifuged, and the supernatant was discarded. The rinsing process was repeated three times. Afterward, the solution of the negatively charged $Fe_{3-\delta}O_4$@PSS NPs was dispersed in 10 mL of PDADMAC, and the mixture was also stirred for 10 min, ultracentrifuged, and washed three times following the same process as presented below. The sample is then named $Fe_{3-\delta}O_4$@(PSS/PDADMAC)$_1$ (the subscript 1 indicates that one bilayer of PSS/PDADMAC is deposited at the surface of the $Fe_{3-\delta}O_4$@NH_3^+). This process was repeated as many times as the desired number of bilayers (PSS/PDADMAC) was reached, which led to $Fe_{3-\delta}O_4$@(PSS/PDADMAC)$_n$, where n is the number of bilayers in the shell.

Characterization. DLS was performed at room temperature using a Malvern Zetasizer HSa instrument with a He−Ne laser (4×10^{-3} W) at a wavelength of 633 nm. NP aqueous solutions were filtered through Millipore membranes (0.2 mm pore size). Data were analyzed by the CONTIN method to obtain the hydrodynamic diameter and size distribution for each aqueous dispersion of NPs. The crystallographic structure of the NPs was identified by XRD using a Philips PW3710 diffractometer with Cu Kα radiation. For TEM observations, one drop of a dispersed solution of NPs was deposited on holey carbon grids and imaged. A transmission electron microscope used was a JEM - ARM 200F Cold FEG TEM/STEM operating at 200 kV and equipped with a spherical aberration (Cs) probe and image correctors. The magnetic properties of the core/shell NPs were studied by a superconducting quantum interference device SQUID-VSM combined to a vibrating sample magnetometer.

Biological Characterization. *Cell Culture.* The THP-1 human monocytic leukemia cell line (ATCC CRL2192; Manassas; USA) was grown in Dulbecco's modified Eagle medium high-glucose (DMEM; Sigma-Aldrich, St. Louis, USA) medium supplemented with 15% fetal bovine serum (FBS), 1% penicillin−streptomycin ,2% L-glutamine, and 0.25 μg mL^{-1} amphotericin B (Sigma-Aldrich, St. Louis, USA). Cells were grown at 37 °C under a 5% CO_2 atmosphere and were passed every 3 days.

https://dx.doi.org/10.1021/acsomega.9b02963
ACS Omega 2020, 5, 4770−4777

Cell Treatment. Cells were seeded in 96 well plates with 5×10^3 cells per well. After overnight incubation, plates were centrifuged ($800 \times g$, 10 min), and the medium with FBS was removed. A fresh medium without FBS and with 0, 1.5, 3.125, 6.25, 12.5, 25, 50, and 100 $\mu g\ mL^{-1}$ each CNM was added, and cells were incubated for 24 and 72 h. Six wells were used per culture condition, and experiments were repeated four times.

WST-1 Assay. The tetrazolium salt 2-(4-iodophenyl)-3-(4nitrophenyl)-5-(2,4-disulfophenyl)-2*H*-tetrazolium, monosodium salt, better known as WST-1 (Roche; Boulogne; France), was used to measure cell viability by detecting the mitochondrial dehydrogenase activity as previously described.[45] Briefly, after treatment, 5 μL of WST-1 was added and incubated for 2 h at 37 °C. Absorbance was measured at 450 nm with a reference wavelength of 690 nm, using an iMarK Microplate Reader (Bio-Rad Laboratories, Osaka, Japan). Inhibitory concentration IC_{50} was calculated by the Reed−Muench formula.[46]

■ ASSOCIATED CONTENT

Supporting Information

The Supporting Information is available free of charge at https://pubs.acs.org/doi/10.1021/acsomega.9b02963.

The presence of characteristic diffraction peaks at 2θ = 30.10, 35.60, 43.14, 53.49, 57.11, and 62.88° at each step of the functionalization process, confirming that the process used for the LbL deposition of the polyelectrolyte did not alter the crystalline structure of the core of the nanoparticles (Figure S1). The complete dispersion of the polyelectrolyte functional nanoparticulate system was confirmed by DLS measurement, and the size (and its polydispersity via the PDI) is illustrated (Figure S2). The superparamagnetic behavior of the NPs was confirmed by ZF-ZFC measurements of NPs at each step of modification. The blocking temperature found to be 270 K (around −3 °C) is higher than those reported for other iron oxide NPs with close sizes, which suggested that the NPs can be slightly aggregated in the physiological media (Figure S3) (PDF)

■ AUTHOR INFORMATION

Corresponding Author

Halima Alem − *Institut Jean Lamour (UMR 7198), Université de Lorraine, CNRS, 54011 Nancy, France; Institut Universitaire de France, 75005 Paris, France;* orcid.org/0000-0002-7918-0504; Email: Halima.alem@univ-lorraine.fr

Authors

Zied Ferjaoui − *Institut Jean Lamour (UMR 7198), Université de Lorraine, CNRS, 54011 Nancy, France*

Sara Nahle − *Institut Jean Lamour (UMR 7198), Université de Lorraine, CNRS, 54011 Nancy, France*

Crosby Soon Chang − *Institut Jean Lamour (UMR 7198), Université de Lorraine, CNRS, 54011 Nancy, France*

Jaafar Ghanbaja − *Institut Jean Lamour (UMR 7198), Université de Lorraine, CNRS, 54011 Nancy, France*

Olivier Joubert − *Institut Jean Lamour (UMR 7198), Université de Lorraine, CNRS, 54011 Nancy, France;* orcid.org/0000-0001-6440-191X

Raphaël Schneider − *Laboratoire Réactions et Génie des Procédés, Université de Lorraine, CNRS, LRGP, 54000 Nancy, France;* orcid.org/0000-0002-6870-6902

Luc Ferrari − *Institut Jean Lamour (UMR 7198), Université de Lorraine, CNRS, 54011 Nancy, France*

Eric Gaffet − *Institut Jean Lamour (UMR 7198), Université de Lorraine, CNRS, 54011 Nancy, France*

Complete contact information is available at: https://pubs.acs.org/10.1021/acsomega.9b02963

Notes

The authors declare no competing financial interest.

■ ACKNOWLEDGMENTS

Financial support has been given by the Centre National de Recherche Scientifique (CNRS) and Institut Universitaire de France.

■ REFERENCES

(1) Shen, B.; Ma, Y.; Yu, S.; Ji, C. Smart Multifunctional Magnetic Nanoparticle-Based Drug Delivery System for Cancer Thermo-Chemotherapy and Intracellular Imaging. *ACS Appl. Mater. Interfaces* **2016**, *8*, 24502−24508.

(2) Bañobre-López, M.; Teijeiro, A.; Rivas, J. Magnetic Nanoparticle-Based Hyperthermia for Cancer Treatment. *Rep. Pract. Oncol. Radiother.* **2013**, *18*, 397−400.

(3) Blanco-Andujar, C.; Walter, A.; Cotin, G.; Bordeianu, C.; Mertz, D.; Felder-Flesch, D.; Begin-Colin, S. Design of Iron Oxide-Based Nanoparticles for MRI and Magnetic Hyperthermia. *Nanomedicine* **2016**, *11*, 1889−1910.

(4) Dias, C. S. B.; Hanchuk, T. D. M.; Wender, H.; Shigeyosi, W. T.; Kobarg, J.; Rossi, A. L.; Tanaka, M. N.; Cardoso, M. B.; Garcia, F. Shape Tailored Magnetic Nanorings for Intracellular Hyperthermia Cancer Therapy. *Sci. Rep.* **2017**, *7*, 14843.

(5) Kandasamy, G.; Maity, D. Recent Advances in Superparamagnetic Iron Oxide Nanoparticles (SPIONs) for in Vitro and in Vivo Cancer Nanotheranostics. *Int. J. Pharm.* **2015**, *496*, 191−218.

(6) Dunn, A. E.; Dunn, D. J.; Lim, M.; Boyer, C.; Thanh, N. T. K. Recent Developments in the Design of Nanomaterials for Photothermal and Magnetic Hyperthermia Induced Controllable Drug Delivery. *NANO* **2013**, 225−254.

(7) Soenen, S. J.; De Cuyper, M. Assessing Iron Oxide Nanoparticle Toxicity in Vitro: Current Status and Future Prospects. *Nanomedicine* **2010**, *5*, 1261−1275.

(8) Macchione, M.; Biglione, C.; Strumia, M. Design, Synthesis and Architectures of Hybrid Nanomaterials for Therapy and Diagnosis Applications. *Polymer* **2018**, *10*, 527.

(9) Zhao, N.; Yan, L.; Zhao, X.; Chen, X.; Li, A.; Zheng, D.; Zhou, X.; Dai, X.; Xu, F.-J. Versatile Types of Organic/Inorganic Nanohybrids: From Strategic Design to Biomedical Applications. *Chem. Rev.* **2019**, *119*, 1666−1762.

(10) Baaziz, W.; Pichon, B. P.; Fleutot, S.; Liu, Y.; Lefevre, C.; Greneche, J.-M.; Toumi, M.; Mhiri, T.; Begin-Colin, S. Magnetic Iron Oxide Nanoparticles: Reproducible Tuning of the Size and Nanosized-Dependent Composition, Defects, and Spin Canting. *J. Phys. Chem. C* **2014**, *118*, 3795−3810.

(11) Gillich, T.; Acikgöz, C.; Isa, L.; Schlüter, A. D.; Spencer, N. D.; Textor, M. PEG-Stabilized Core−Shell Nanoparticles: Impact of Linear versus Dendritic Polymer Shell Architecture on Colloidal Properties and the Reversibility of Temperature-Induced Aggregation. *ACS Nano* **2013**, *7*, 316−329.

(12) Jamal Al Dine, E.; Ferjaoui, Z.; Ghanbaja, J.; Roques-Carmes, T.; Meftah, A.; Hamieh, T.; Toufaily, J.; Schneider, R.; Marchal, S.; Gaffet, E.; et al. Thermo-Responsive Magnetic Fe_3O_4@P(MEO_2MA_X−OEGMA$_{100-X}$) NPs and Their Applications as Drug Delivery Systems. *Int. J. Pharm.* **2017**, *532*, 738−747.

(13) Palomec-Garfias, A. F.; Jardim, K. V.; Sousa, M. H.; Márquez-Beltrán, C. Influence of Polyelectrolyte Chains on Surface Charge and Magnetization of Iron Oxide Nanostructures. *Colloids Surf., A* **2018**, *549*, 13−24.
(14) Zhang, Z.-Q.; Song, S.-C. Thermosensitive/Superparamagnetic Iron Oxide Nanoparticle-Loaded Nanocapsule Hydrogels for Multiple Cancer Hyperthermia. *Biomaterials* **2016**, *106*, 13−23.
(15) He, R.; You, X.; Shao, J.; Gao, F.; Pan, B.; Cui, D. Core/Shell Fluorescent Magnetic Silica-Coated Composite Nanoparticles for Bioconjugation. *Nanotechnology* **2007**, *18*, 315601.
(16) Yang, P.; Quan, Z.; Hou, Z.; Li, C.; Kang, X.; Cheng, Z.; Lin, J. A Magnetic, Luminescent and Mesoporous Core−Shell Structured Composite Material as Drug Carrier. *Biomaterials* **2009**, *30*, 4786−4795.
(17) Arami, H.; Khandhar, A. P.; Tomitaka, A.; Yu, E.; Goodwill, P. W.; Conolly, S. M.; Krishnan, K. M. In Vivo Multimodal Magnetic Particle Imaging (MPI) with Tailored Magneto/Optical Contrast Agents. *Biomaterials* **2015**, *52*, 251−261.
(18) Dine, E. J. A.; Ferjaoui, Z.; Roques-Carmes, T.; Schjen, A.; Meftah, A.; Hamieh, T.; Toufaily, J.; Schneider, R.; Gaffet, E.; Alem, H. Efficient Synthetic Access to Thermo-Responsive Core/Shell Nanoparticles. *Nanotechnology* **2017**, *28*, 125601.
(19) Sun, Q.; Cheng, D.; Yu, X.; Zhang, Z.; Dai, J.; Li, H.; Liang, B.; Shuai, X. A pH-Sensitive Polymeric Nanovesicle Based on Biodegradable Poly(Ethylene Glycol)-*b*-Poly(2-(Diisopropylamino)-Ethyl Aspartate) as a MRI-Visible Drug Delivery System. *J. Mater. Chem.* **2011**, *21*, 15316−15326.
(20) Thorat, N. D.; Bohara, R. A.; Malgras, V.; Tofail, S. A. M.; Ahamad, T.; Alshehri, S. M.; Wu, K. C.-W.; Yamauchi, Y. Multimodal Superparamagnetic Nanoparticles with Unusually Enhanced Specific Absorption Rate for Synergetic Cancer Therapeutics and Magnetic Resonance Imaging. *ACS Appl. Mater. Interfaces* **2016**, *8*, 14656−14664.
(21) Thorat, N. D.; Bohara, R. A.; Noor, M. R.; Dhamecha, D.; Soulimane, T.; Tofail, S. A. M. Effective Cancer Theranostics with Polymer Encapsulated Superparamagnetic Nanoparticles: Combined Effects of Magnetic Hyperthermia and Controlled Drug Release. *ACS Biomater. Sci. Eng.* **2017**, *3*, 1332−1340.
(22) Al Dine, E. J.; Marchal, S.; Schneider, R.; Hamie, B.; Ghanbaja, J.; Roques-Carmes, T.; Hamieh, T.; Toufaily, J.; Gaffet, E.; Alem, H. A Facile Approach for Doxorubicine Delivery in Cancer Cells by Responsive and Fluorescent Core/Shell Quantum Dots. *Bioconjugate Chem.* **2018**, *29*, 2248−2256.
(23) Ferjaoui, Z.; Schneider, R.; Meftah, A.; Gaffet, E.; Alem, H. Functional Responsive Superparamagnetic Core/Shell Nanoparticles and Their Drug Release Properties. *RSC Adv.* **2017**, *7*, 26243−26249.
(24) Decher, G.; Schlenoff, J. B. *Multilayer Thin Films: Sequential Assembly of Nanocomposite Materials*; John Wiley & Sons: 2012.
(25) Arys, X.; Laschewsky, A.; Jonas, A. M. Ordered Polyelectrolyte "Multilayers". 1. Mechanisms of Growth and Structure Formation: A Comparison with Classical Fuzzy "Multilayers". *Macromolecules* **2001**, *34*, 3318−3330.
(26) Alorabi, A. Q.; Tarn, M. D.; Gómez-Pastora, J.; Bringas, E.; Ortiz, I.; Paunov, V. N.; Pamme, N. On-Chip Polyelectrolyte Coating onto Magnetic Droplets − towards Continuous Flow Assembly of Drug Delivery Capsules. *Lab Chip* **2017**, *17*, 3785−3795.
(27) Ariga, K.; Lvov, Y. M.; Kawakami, K.; Ji, Q.; Hill, J. P. Layer-by-Layer Self-Assembled Shells for Drug Delivery. *Adv. Drug Delivery Rev.* **2011**, *63*, 762−771.
(28) Parakhonskiy, B. V.; Yashchenok, A. M.; Möhwald, H.; Volodkin, D.; Skirtach, A. G. Release from Polyelectrolyte Multilayer Capsules in Solution and on Polymeric Surfaces. *Adv. Mater. Interfaces* **2017**, *4*, 1600273.
(29) Rivera-Gil, P.; De Koker, S.; De Geest, B. G.; Parak, W. J. Intracellular Processing of Proteins Mediated by Biodegradable Polyelectrolyte Capsules. *Nano Lett.* **2009**, *9*, 4398−4402.
(30) Sukhorukov, G. B.; Rogach, A. L.; Zebli, B.; Liedl, T.; Skirtach, A. G.; Köhler, K.; Antipov, A. A.; Gaponik, N.; Susha, A. S.; Winterhalter, M.; et al. Nanoengineered Polymer Capsules: Tools for Detection, Controlled Delivery, and Site-Specific Manipulation. *Small* **2005**, *1*, 194−200.
(31) Santos, J. P.; Welsh, E. R.; Gaber, B. P.; Singh, A. Polyelectrolyte-Assisted Immobilization of Active Enzymes on Glass Beads. *Langmuir* **2001**, *17*, 5361−5367.
(32) Volodkin, D. $CaCO_3$ Templated Micro-Beads and -Capsules for Bioapplications. *Adv. Colloid Interface Sci.* **2014**, *207*, 306−324.
(33) Wang, Y.; Yu, A.; Caruso, F. Nanoporous Polyelectrolyte Spheres Prepared by Sequentially Coating Sacrificial Mesoporous Silica Spheres. *Angew. Chem. Int. Ed.* **2005**, *44*, 2888−2892.
(34) Yang, Y.-J.; Tao, X.; Hou, Q.; Ma, Y.; Chen, X.-L.; Chen, J.-F. Mesoporous Silica Nanotubes Coated with Multilayered Polyelectrolytes for PH-Controlled Drug Release. *Acta Biomater.* **2010**, *6*, 3092−3100.
(35) Caruso, F. Hollow Capsule Processing through Colloidal Templating and Self-Assembly. *Chem. − Eur. J.* **2000**, *6*, 413−419.
(36) Gil, P. R.; del Mercato, L. L.; del _Pino, P.; Muñoz_Javier, A.; Parak, W. J. Nanoparticle-Modified Polyelectrolyte Capsules. *Nano Today* **2008**, *3*, 12−21.
(37) Lu, Z.; Prouty, M. D.; Guo, Z.; Golub, V. O.; Kumar, C. S. S. R.; Lvov, Y. M. Magnetic Switch of Permeability for Polyelectrolyte Microcapsules Embedded with Co@Au Nanoparticles. *Langmuir* **2005**, *21*, 2042−2050.
(38) Shchukin, D. G.; Radtchenko, I. L.; Sukhorukov, G. B. Micron-Scale Hollow Polyelectrolyte Capsules with Nanosized Magnetic Fe3O4 Inside. *Mater. Lett.* **2003**, *57*, 1743−1747.
(39) Mancarella, S.; Greco, V.; Baldassarre, F.; Vergara, D.; Maffia, M.; Leporatti, S. Polymer-Coated Magnetic Nanoparticles for Curcumin Delivery to Cancer Cells. *Macromol. Biosci.* **2015**, *15*, 1365−1374.
(40) Wong, J. E.; Gaharwar, A. K.; Müller-Schulte, D.; Bahadur, D.; Richtering, W. Magnetic Nanoparticle−Polyelectrolyte Interaction: A Layered Approach for Biomedical Applications. *J. Nanosci. Nanotechnol.* **2008**, *8*, 4033−4040.
(41) Chen, J.; Lin, Y.; Jia, L. Preparation of Anionic Polyelectrolyte Modified Magnetic Nanoparticles for Rapid and Efficient Separation of Lysozyme from Egg White. *J. Chromatogr. A* **2015**, *1388*, 43−51.
(42) Cristofolini, L.; Szczepanowicz, K.; Orsi, D.; Rimoldi, T.; Albertini, F.; Warszynski, P. Hybrid Polyelectrolyte/Fe3O4 Nanocapsules for Hyperthermia Applications. *ACS Appl. Mater. Interfaces* **2016**, *8*, 25043−25050.
(43) Schönhoff, M. Layered Polyelectrolyte Complexes: Physics of Formation and Molecular Properties. *J. Phys. Condens. Matter* **2003**, *15*, R1781.
(44) Alem, H.; Schejn, A.; Roques-Carmes, T.; Ghanbaja, J.; Schneider, R. Thermo-Responsive and Aqueous Dispersible ZnO/PNIPAM Core/Shell Nanoparticles. *Nanotechnology* **2015**, *26*, 335605.
(45) Nahle, S.; Safar, R.; Grandemange, S.; Foliguet, B.; Lovera-Leroux, M.; Doumandji, Z.; le Faou, A.; Joubert, O.; Rihn, B.; Ferrari, L. Single Wall and Multiwall Carbon Nanotubes Induce Different Toxicological Responses in Rat Alveolar Macrophages. *J. Appl. Toxicol.* **2019**, *39*, 764−772.
(46) Ramakrishnan, M. A. Determination of 50% Endpoint Titer Using a Simple Formula. *World J. Virol.* **2016**, *5*, 85.
(47) Laurent, S.; Forge, D.; Port, M.; Roch, A.; Robic, C.; Vander Elst, L.; Muller, R. N. Magnetic Iron Oxide Nanoparticles: Synthesis, Stabilization, Vectorization, Physicochemical Characterizations, and Biological Applications. *Chem. Rev.* **2008**, *108*, 2064−2110.
(48) Sukhanova, A.; Bozrova, S.; Sokolov, P.; Berestovoy, M.; Karaulov, A.; Nabiev, I. Dependence of Nanoparticle Toxicity on Their Physical and Chemical Properties. *Nanoscale Res. Lett.* **2018**, *13*, 44.
(49) Lara, S.; Perez-Potti, A.; Herda, L. M.; Adumeau, L.; Dawson, K. A.; Yan, Y. Differential Recognition of Nanoparticle Protein Corona and Modified Low-Density Lipoprotein by Macrophage Receptor with Collagenous Structure. *ACS Nano* **2018**, *12*, 4930−4937.

https://dx.doi.org/10.1021/acsomega.9b02963
ACS Omega 2020, 5, 4770−4777

(50) Li, Z.; Yuan, D.; Jin, G.; Tan, B. H.; He, C. Facile Layer-by-Layer Self-Assembly toward Enantiomeric Poly(Lactide) Stereocomplex Coated Magnetite Nanocarrier for Highly Tunable Drug Deliveries. *ACS Appl. Mater. Interfaces* **2016**, *8*, 1842−1853.
(51) Spasova, M.; Salgueiriño-Maceira, V.; Schlachter, A.; Hilgendorff, M.; Giersig, M.; Liz-Marzán, L. M.; Farle, M. Magnetic and Optical Tunable Microspheres with a Magnetite/Gold Nanoparticle Shell. *J. Mater. Chem.* **2005**, *15*, 2095.
(52) Fröhlich, E. The Role of Surface Charge in Cellular Uptake and Cytotoxicity of Medical Nanoparticles. *Int. J. Nanomedicine* **2012**, *7*, 5577−5591.
(53) Schönhoff, M. Self-Assembled Polyelectrolyte Multilayers. *Curr. Opin. Colloid Interface Sci.* **2003**, *8*, 86−95.
(54) Gupta, A. K.; Gupta, M. Synthesis and Surface Engineering of Iron Oxide Nanoparticles for Biomedical Applications. *Biomaterials* **2005**, *26*, 3995−4021.
(55) Huang, J.; Wang, L.; Zhong, X.; Li, Y.; Yang, L.; Mao, H. Facile Non-Hydrothermal Synthesis of Oligosaccharide Coated Sub-5 Nm Magnetic Iron Oxide Nanoparticles with Dual MRI Contrast Enhancement Effects. *J. Mater. Chem. B* **2014**, *2*, 5344−5351.
(56) Gloria, A.; Russo, T.; D'Amora, U.; Zeppetelli, S.; D'Alessandro, T.; Sandri, M.; Bañobre-López, M.; Piñeiro-Redondo, Y.; Uhlarz, M.; Tampieri, A.; et al. Magnetic Poly(ε-Caprolactone)/Iron-Doped Hydroxyapatite Nanocomposite Substrates for Advanced Bone Tissue Engineering. *J. R. Soc., Interface* **2013**, *10*, 20120833−20120833.
(57) Chanput, W.; Mes, J. J.; Wichers, H. J. THP-1 Cell Line: An in Vitro Cell Model for Immune Modulation Approach. *Int. Immunopharmacol.* **2014**, *23*, 37−45.
(58) Mizuno, K.; Toyoda, Y.; Fukami, T.; Nakajima, M.; Yokoi, T. Stimulation of Pro-Inflammatory Responses by Mebendazole in Human Monocytic THP-1 Cells through an ERK Signaling Pathway. *Arch. Toxicol.* **2011**, *85*, 199−207.
(59) Alarifi, S.; Ali, D.; Alkahtani, S.; Alhader, M. S. Iron Oxide Nanoparticles Induce Oxidative Stress, DNA Damage, and Caspase Activation in the Human Breast Cancer Cell Line. *Biol. Trace Elem. Res.* **2014**, *159*, 416−424.
(60) Khan, M. I.; Mohammad, A.; Patil, G.; Naqvi, S. A. H.; Chauhan, L. K. S.; Ahmad, I. Induction of ROS, Mitochondrial Damage and Autophagy in Lung Epithelial Cancer Cells by Iron Oxide Nanoparticles. *Biomaterials* **2012**, *33*, 1477−1488.

https://dx.doi.org/10.1021/acsomega.9b02963
ACS Omega 2020, 5, 4770−4777